A physical model of sound diffraction and reflections in the human concha

Enrique A. Lopez-Poveda and Ray Meddis
Hearing Research Laboratory, Department of Psychology, Essex University, Colchester CO4 3SQ, United Kingdom

(Received 25 May 1995; revised 15 March 1996; accepted 5 June 1996)

An approximated physical model of the frequency transfer function of the human concha is developed in this paper. This formulation includes diffraction, reflection, and interference phenomena in the concha cavity. The performance of the proposed diffraction/reflection model is compared with that of the single-delay-and-add approximation by checking their predictions against the experimental transfer function of a metal spiral-shaped diffracting/reflecting system. Results show that the diffraction/reflection model performs considerably better at predicting both the absolute center frequency of spectral minima and the relative frequency spacing between them. The diffraction/reflection model is then applied to a realistic concha shape and its predictions are compared with experimental head-related transfer functions for azimuth- and elevation-varying sound sources. In this case, the model predicts the elevation-dependent spectral features related to the transverse dimensions of the concha. Additionally, the diffraction/reflection model predicts that, because of sound diffraction, similar spectral features must be generated in the concha for sources at all azimuths within the frontal part of the ipsilateral hemisphere. Experimental and theoretical evidence supporting this prediction is presented.

PACS numbers: 43.64.Ha, 43.66.Qp [RDF]

LIST OF SYMBOLS

Note: This list only contains variables that have not been defined in the main text. Complex magnitudes have been written in bold characters, e.g., $\mathbf{p_0}$. A small bar on the character indicates vectorial notation, e.g., k. Figure 1(a) illustrates some of these magnitudes.

ϕ	angle of elevation, (being 0° elevation when the sound source is placed in front of the subject at the eye level, +90° elevation when the source is vertically above and −90° is when the sound source is vertically below)
f	frequency
t	time
$\mathbf{p_T}$	total pressure at the meatus entrance
$\mathbf{p_R}$	reflected pressure from the concha wall measured at the meatus entrance
$\mathbf{p_U}$	$=\mathbf{p_T}-\mathbf{p_R}$
$\mathbf{p_0}(\overline{r},t)$	incident sound pressure at point $\overline{r}$
P_0	amplitude of the incident sound wave
$\mathbf{p}_0$	incident sound pressure at the origin ($\overline{r}=0$)
ω	angular frequency; $\omega=2\pi f$
k	wave vector; $k=2\pi/\lambda$
λ	wavelength
j	$=\sqrt{-1}$
$\overline{n_l}$	unit vector normal to the diffracting aperture
$\overline{n_q}$	unit vector normal to the reflecting surface
$\overline{\mathbf{u}}(\overline{r},t)$	particle velocity at point $\overline{r}$, defined as $\overline{\mathbf{u}}(\overline{r},t)=-(1/\rho)\int\nabla\mathbf{p}(\overline{r},t)dt$ (Morse and Ingard, 1968)
ρ	density of the propagating medium
c	speed of sound (we have considered $c=332.1$ m/s)
S_A	surface of the diffracting aperture
S_R	reflecting surface

INTRODUCTION

Accurate sound localization is a complex task which requires the availability of many cues. Interaural time differences, interaural level differences, head movements, and spectral cues originated by the direction-dependent filtering of the pinnae are some of these cues. It is now understood that interaural time differences and interaural level differences are not enough by themselves to encode unambiguously the position of the sound source in space (Mills, 1972). Therefore, in a situation where the head and the source are stationary, the only remaining localization cue to resolve the ''cone of confusion'' described by Mills is provided by the direction-dependent spectral filtering of the pinnae. In particular, spectral features constitute the only available information for localizing sounds placed in the median vertical plane.

The main spectral features (peaks and notches) produced by the direction-dependent filtering of the pinna have been described by Shaw and Teranishi (1968). The dependence of the external ear's transfer function on azimuth and on elevation has also been well characterized using mechanical models of the ear (Teranishi and Shaw, 1968; Shaw, 1975). These latter studies permitted identification of the physical cause of most of the spectral peaks measured at the eardrum position for incident flat-spectrum broadband signals. However, the physical cause of some remarkable spectral notches remains unclear. In particular, Shaw and Teranishi (1968)

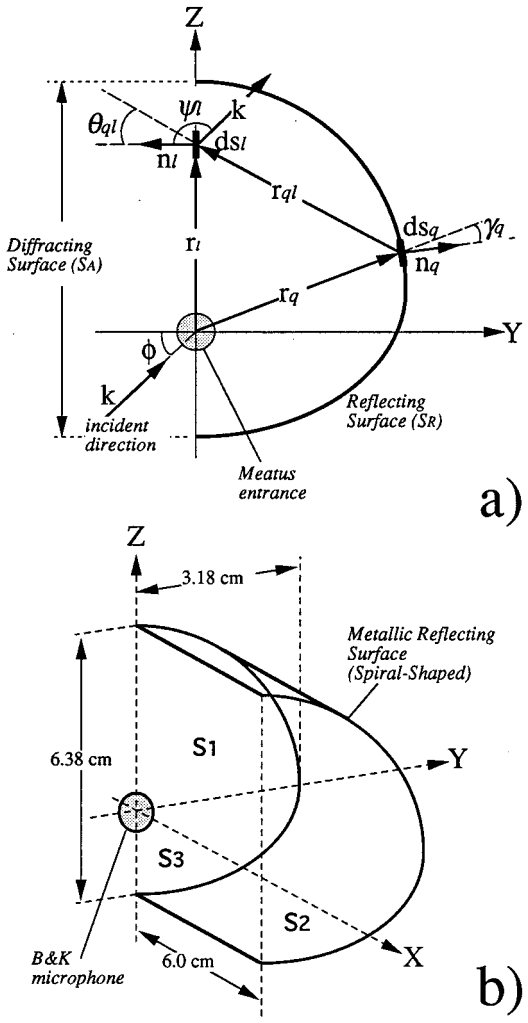

FIG. 1. (a) A two-dimensional view of the geometry of the problem and the convention taken for the definition of the different variables involved. (b) Experimental setup and dimensions of the reflecting spiral-shaped surface.

described a sharp minimum whose central frequency seems to vary from 6.5 kHz at −45° elevation to frequencies above 10 kHz for +45° elevation in the lateral plane. Unfortunately, they were unable, at that time, to give a proven explanation for such a prominent feature.

The importance of spectral minima as sound localization cues in the median vertical plane is supported by the perceptual studies performed by Hebrank and Wright (1974). They concluded that elevation in the median vertical plane (−45° to +45° elevation) is cued by a spectral notch whose central frequency has the same dependence on elevation as that previously observed by Shaw and Teranishi (1968) in the lateral plane. Further results have confirmed this conclusion in both the median vertical plane (Butler and Belendiuk, 1977) and in the lateral vertical plane (Bloom, 1977).

Clearly, if the incident undisturbed signal has a flat spectrum, spectral notches must be caused necessarily by destructive interference at the meatus entrance (Shaw and Teranishi, 1968). According to Batteau's theory of pinna reflections (Batteau, 1967), interference between the direct wave and the reflected wave from the whole of the pinna could be responsible for them. However, Hebrank and Wright (1974) hypothesized that reflections from the posterior wall of the concha alone may be responsible for the observed notch in the median plane. In an attempt to evaluate the validity of this statement, Hebrank and Wright regarded the human concha as a single-delay-and-add system where the elevation-dependent delay, $\tau(\phi)$, between the direct sound entering the meatus and the reflected sound from the concha's posterior wall is related to the extra path, or path difference (d), traveled by the reflected wave. The relation is as follows: $\tau(\phi) = d/c$. For sound sources in the median plane, each elevation angle would generate a particular value of d and thus a different delay. Since a single path difference is considered by this reflection theory, it implies that reflection occurs at a single point on the concha's posterior wall. The single-delay-and-add formulation provides a discrete collection of notch frequencies given by the expression $f_n = n[1/2\tau(\phi)]$ ($n = 1,3,5,\ldots$).

Despite the simplicity of the single-delay-and-add model, its predictions indicate that reflections from the posterior wall of the concha may be responsible for the production of the elevation-dependent spectral notch in the median vertical plane. However, a satisfactory explanation as to why a similar elevation-dependent notch has been also observed for incident sounds from the lateral vertical plane [Shaw and Teranishi, 1968; Bloom, 1977; Carlile and Pralong, 1994, Fig. 5(b)] cannot be intuitively inferred from the mechanics of the concha reflections model explained above. For incident sounds from the lateral vertical plane, the concha posterior wall is parallel to the direction of incidence and, therefore, reflections from the posterior wall of the concha are not obvious. Despite this, it is observed that the center frequency and the elevation-dependent behavior of the notch in question are similar when the sound source is placed in the median and the lateral vertical planes (additional experimental data supporting this experimental observation is presented below) as though they were caused by the same mechanism.

The aim of the work presented in this paper is to investigate a theoretical explanation for some of the spectral features (peaks and notches) observed in experimental head-related transfer functions (Shaw and Teranishi, 1968; Hebrank and Wright, 1974; Butler and Belendiuk, 1977; Mehrgardt and Mellert, 1977; Carlile and Pralong, 1994; Pralong and Carlile, 1994), in particular those caused by the concha. Special attention is dedicated to the characteristic elevation-dependent spectral notch described above. The basic hypothesis that guides our approach is that the elevation-dependent notch observed for incident sounds from both the lateral and median vertical planes is caused by cancellation between the direct wave entering the meatus and the sound reflected from the concha posterior wall. However, sound diffraction is necessary to explain how similar reflections on the posterior wall of concha occur in both cases. In our view, the sound wave is diffracted (scattered within the concha) as it enters the concha cavity and, therefore, significant reflections must occur on an infinite number of points along the posterior wall for all source locations.

To test our hypothesis we have developed a model to simulate the spectral features related to the transverse geometry of the concha cavity. The model is inspired by the idea

of concha reflections proposed by Hebrank and Wright (1974) but includes sound diffraction in the concha aperture as well as reflections on a large number of points on the concha posterior wall. Under certain assumptions and geometrical approximations an attempt is made to develop the model in the frequency domain from simple physical principles. The predictions of the diffraction/reflection model are then tested against experimental measurements for an ideal diffracting/reflecting system with a spiral shape [Fig. 1(b)]. The predictions of the diffraction/reflection model regarding the position of spectral notches are quantitatively compared with the predictions of the single-delay-and-add model for this simple geometry.

The proposed diffraction/reflection model is also applied to a more realistic three-dimensional conchalike shape (see below) in an attempt to simulate the spectral features (peaks and notches) generated by the transverse dimensions of the concha. For the latter case, the diffraction/reflection model predicts a spectral notch which shows a dependence on azimuth (Shaw and Teranishi, 1968; Mehrgardt and Mellert, 1977; Pralong and Carlile, 1994; Carlile and Pralong, 1994) and elevation (Shaw and Teranishi, 1968; Hebrank and Wright, 1974; Shaw, 1975; Butler and Belendiuk, 1977; Carlile and Pralong, 1994) similar to the notch observed by Hebrank and Wright. Additionally, model results suggest that secondary notches occurring at higher frequencies within the audible range are also caused by the same diffraction/reflection process in the concha.

I. THEORY

An exact expression for the transfer function of any acoustic system requires the wave equation to be solved (generally by numerical methods), with the right boundary conditions for the geometry of the system. Even for objects with simple geometry and well-determined acoustic characteristics, the process of solving the wave equation is nontrivial and computationally very expensive (Filippi and Dumery, 1969; Cassot, 1975; Martin and Rizzo, 1989). This is true particularly for an acoustic system such as the human ear. For these reasons we have restricted our analysis to the human concha and opted for an *approximated* approach to obtain its transfer function. The approximations and assumptions made in our approach are listed below. Obviously, since some approximations are required, the final transfer function is inexact. However, the proposed approximated transfer function can help us understand a great deal about the mechanisms which generate some of the most characteristic spectral features observed in experimental head-related transfer functions.

A. General

Because the dimensions of the concha aperture are comparable to audible sound wavelengths, the incident wave will be diffracted as it enters the concha cavity. Hence, it will spread within the cavity following the rules of diffraction. The diffracted wave will then be reflected from the wall of the concha. It is convenient to express the total sound pressure at the ear canal entrance as the sum of the direct unreflected pressure from the concha aperture plus the reflected pressure from the concha reflecting wall, i.e.,

$$\mathbf{p_T} = \mathbf{p_U} + \mathbf{p_R}. \tag{1}$$

In the frequency domain, the transfer function of the concha can be expressed as the ratio of the total pressure at the meatus entrance over the value that the incident wave would have at the same point if the concha was not present. Mathematically, the transfer function of the concha can be written as follows:

$$\frac{\mathbf{p_T}}{\mathbf{p_0}} = \frac{\mathbf{p_U} + \mathbf{p_R}}{\mathbf{p_0}}. \tag{2}$$

As it will be explained below, the phase of the total pressure at the meatus entrance has a directional contribution which depends on the location of the sound. Therefore, the above transfer function should predict some of the spectral transformations introduced by the concha as a function of source position.

B. Theoretical approximations and assumptions

Both magnitudes, $\mathbf{p_U}$ and $\mathbf{p_R}$, clearly depend on the shapes of the concha reflecting wall and the concha aperture which are extremely complicated and vary substantially across subjects. In order to simplify the problem, a few general approximations and assumptions regarding the geometry of the system have been made. In addition, the general diffraction theories used in the proposed model do not apply specifically for apertures with dimensions much smaller than the wavelength. Therefore, some assumptions need to be made so that those theories can also be applied in our case. These general approximations and assumptions are:

(i) The ratio $\mathbf{p_U}/\mathbf{p_0}$ is approximated to 1. This is not strictly true, but it may be justified by the fact that the distance from the concha aperture to the meatus entrance is very small compared to the minimum wavelength ($\approx$1.8 cm) of the considered sounds (1 Hz to 17 kHz).

(ii) It will be assumed that the concha entrance is a two-dimensional aperture on an infinitely large sound-opaque screen. This approximation is convenient because it allows the application of Kirchhoff's theory of diffraction by an aperture (Ditchburn, 1976; Hecht, 1990) to specify the diffracted pressure at any point within the concha cavity (particularly at points on the reflecting surface).

(iii) For frequencies below around 6 kHz the wavelength can be much larger than both the dimensions of the concha aperture and the distances between it and the concha reflecting wall. Therefore, for frequencies lower than 6 kHz, Kirchhoff's diffraction theory is inappropriate to find the diffracted pressure at points within the concha cavity. Nevertheless, we have tentatively tested the diffraction/reflection model based on Kirchhoff's theory for lower frequencies and found that, if approximation (i) is made, reasonable predictions are obtained even at these lower frequencies.

(iv) It will be approximated that the incident pressure on each element of reflecting surface is only given by the diffracted sound impinging directly from the concha aperture. In other words, the contributions from other reflecting

elements to the incident pressure on each reflecting differential have not been considered. The effects of this approximation on the predicted spectra will be discussed below.

(v) If the sound source is placed at least 1 m away from the concha entrance, the pressure wave reaching the concha entrance can be approximated by a plane wave of the form

$$\mathbf{p_0}(\overline{r},t)=P_0\ \exp[j(\overline{k}\cdot\overline{r}-\omega t)]. \tag{3}$$

If we choose a system of coordinates such that its origin is defined at the center of the meatus entrance [see Fig. 1(a)], the value of the undisturbed incident plane wave at this point reduces to

$$\mathbf{p_0}=P_0\ \exp(-j\omega t). \tag{4}$$

(vi) For convenience, we have chosen the center of the meatus entrance as the observation point. A more rigorous approach would consider the effect that longitudinal and transverse modes of resonance within the ear canal have on the experimental head-related transfer functions (Shaw, 1975).

Under approximation (i), the expression for the transfer function of the concha becomes

$$\frac{\mathbf{p_T}}{\mathbf{p_0}}=1+\frac{\mathbf{p_R}}{\mathbf{p_0}}. \tag{5}$$

To obtain a final expression for the concha transfer function, only the ratio $\mathbf{p_R}/\mathbf{p_0}$ needs to be calculated. Unfortunately, $\mathbf{p_R}$ cannot be derived in a trivial manner because the incident pressure on the reflecting wall is the diffracted pressure from the concha aperture. Therefore, the diffracted pressure at any point on the concha wall must be found before attempting to derive an expression for the reflected pressure at the meatus entrance.

C. Diffracted pressure at any point on the concha reflecting wall

Under approximations (ii), (iii), and (iv), the incident pressure at any point $\overline{r_q}$ on the concha reflecting wall [see Fig. 1(a)] can be calculated using Kirchhoff's scalar diffraction theory (Braddick, 1965; Ditchburn, 1976; for a complete review on diffraction phenomena see Hecht, 1990) for a two-dimensional aperture on an opaque screen and an incident plane wave. According to Kirchhoff's theory, each differential of surface in the concha aperture, ds_l, can be seen as a secondary radiator emitting a spherical wave whose value at the point $\overline{r_q}$ on the reflecting surface is given by the expression

$$d\mathbf{p_D}(\overline{r_q},t)=\frac{\mathbf{K}(\theta_{ql},\psi_l,r_{ql})P_0}{r_{ql}}\exp[j(kr_{ql}-\pi/2)+\varphi_l]\exp(-j\omega t)ds_l. \tag{6}$$

When the direction of propagation of the incident plane wave [Eq. (3)] is not normal to the concha aperture [i.e., when the *angle* $(k,\overline{r_l})$ is different from 90°], each secondary radiator on the aperture, ds_l, radiates with an initial phase, φ_l, given by

$$\varphi_l=j\overline{k}\cdot\overline{r_l}, \tag{7}$$

where $\overline{r_l}$ is vector position of the lth surface differential, ds_l. Note that k is the wave vector of the incident plane wave and, therefore, the direction of incidence (i.e., source position) is implicit in the value of its components.

For an incident plane wave, the *diffraction obliquity factor* $\mathbf{K}(\theta_{ql},\psi_l,r_{ql})$, introduced by Kirchhoff's theory is given by

$$\mathbf{K}(\theta_{ql},\psi_l,r_{ql})=\left[\frac{1}{\lambda}\left(\frac{\cos\theta_{ql}-\cos\psi_l}{2}\right)+j\frac{\cos\theta_{ql}}{4\pi r_{ql}}\right] \tag{8}$$

(see the Appendix). It introduces the fact that each surface differential on the aperture ds_l does not radiate with the same amplitude in all directions. The maximum radiation occurs in the direction of propagation of the incident plane wave, i.e., when $\theta_{ql}=\text{angle}(\overline{r_{ql}},\overline{n_l})$ equals zero and $\psi_l=\text{angle}(k,\overline{n_l})$ equals 180° (note that $\overline{n_l}$ is a vector normal to the aperture surface at the position $\overline{r_l}$ and, therefore is defined outward-pointing on the aperture).

The total diffracted pressure incident on any point $\overline{r_q}$ of the reflecting wall is, therefore, obtained by integrating Eq. (6) over the whole of the concha aperture, S_A, i.e.,

$$\mathbf{p_D}(\overline{r_q},t)=\int\int_{S_A}\frac{\mathbf{K}(\theta_{ql},\psi_l,r_{ql})P_0}{r_{ql}}\exp[j(kr_{ql}-\pi/2)+\varphi_l]\exp(-j\omega t)\ ds_l. \tag{9}$$

D. Reflected pressure at the meatus entrance

The next step is to find the pressure at the meatus entrance due to all the waves which have been reflected once. In this case, the same principle used to derive Kirchhoff's expression for the diffracted pressure [Eq. (6)] is used to obtain the reflected pressure, although with the appropriate boundary conditions (see the Appendix). To illustrate the theory in a simple manner, each differential of reflecting surface, ds_q, can be seen as a point reflector which emits a wave whose value at the meatus entrance is given by

$$d\mathbf{p_R}=\frac{\mathbf{R}(r_q,\gamma_q)\mathbf{p_D}(\overline{r_q})}{r_q}\exp(jkr_q-j\omega t)\ ds_q, \tag{10}$$

where r_q is the distance from the reflector ds_q to the meatus entrance. The amplitude with which each ds_q radiates is proportional to the amplitude of the spatial part of the diffracted pressure at ds_q; i.e., proportional to $\mathbf{p_D}(\overline{r_q})$.

If total reflection is assumed, the proportionality factor, $\mathbf{R}(r_q,\gamma_q)$, can be expressed as (see the Appendix)

$$\mathbf{R}(r_q,\gamma_q)=\frac{\cos\gamma_q}{4\pi}\left(-jk+\frac{1}{r_q}\right), \tag{11}$$

where $\gamma_q=\text{angle}(\overline{r_q},\overline{n_q})$ [see Fig. 1(a)]. Notice that $\mathbf{R}(r_q,\gamma_q)$ acts like a directional factor for reflection; it allows maximum reflection in the normal direction to the reflecting surface (i.e., when the angle γ_q is zero) and produces no reflected pressure from points at which γ_q equals 90°. If total reflection is not assumed, the form of $\mathbf{R}(r_q,\gamma_q)$ will be slightly different (see the Appendix) so that it includes the acoustic properties of the reflecting surface.

Substituting the value of $\mathbf{p_D}$ into Eq. (10), operating and integrating over the whole reflecting surface S_R, we can obtain the reflected sound pressure at the meatus entrance, which is given by the expression

$$\mathbf{p_R} = \int_{S_R}\int \int_{S_A}\int \frac{\mathbf{R}(r_q,\gamma_q)\mathbf{K}(\theta_{ql},\psi_l,r_{ql})P_0}{r_q r_{ql}} \times \exp\{j[k(r_q+r_{ql})-\pi/2]+\varphi_l\} \times \exp(-j\omega t)\, ds_l\, ds_q. \quad (12)$$

E. The transfer function of the concha

Finally, substituting Eqs. (4) and (12) into Eq. (5) and operating, a final expression for the transfer function of the concha is obtained:

$$\frac{\mathbf{p_T}}{\mathbf{p_0}} = 1 + \int_{S_R}\int \int_{S_A}\int \frac{\mathbf{R}(r_q,\gamma_q)\mathbf{K}(\theta_{ql},\psi_l,r_{ql})}{r_q r_{ql}} \times \exp\{j[k(r_q+r_{ql})-\pi/2]+\varphi_l\}\, ds_l\, ds_q. \quad (13)$$

It is important to notice that only the variables φ_l and ψ_l depend on the direction of incidence of the sound (i.e., on the source location). The rest of the variables only depend on the geometry of the diffracting/reflecting system.

An analytical solution of the above integral depends strongly on the shape of the concha which needs to be a regular mathematical function in order to express ds_q and ds_l in terms of $\overline{r_q}$, $\overline{r_l}$, and $\overline{r_{ql}}$. However, real concha shapes are irregular and variable among individuals. The numerical evaluation of the transfer function is, on the other hand, more convenient and generalizable to almost any smooth concave shape given by any discrete collection of surface elements. A vectorial approach can be used to relate $\overline{r_q}$, $\overline{r_l}$, and $\overline{r_{ql}}$, and also to find the values of θ_{ql}, ψ_l and γ_q [see Fig. 1(a)].

II. VALIDATION OF THE THEORY

In order to test the formulation presented above for a simple geometry, the frequency transfer function of a spiral-shaped stainless-steel reflecting surface [see Fig. 1(b)] was measured. The predictions of the diffraction/reflection model for the same three-dimensional spiral shape were then compared with the experimental data.

A. Experimental method

The impulse response of a spiral-shaped stainless-steel reflecting surface with a Bruel & Kjaer microphone (model 4134, 1/2 in. condenser mic.) placed at the position[1] indicated in Fig. 1(b) was recorded for three elevations of the sound source ($-45°$, $-17°$, and $+35°$). The measurements were made under *quasi*-free-field conditions and the recording time was set short enough to ensure that no reflected sound from any undesired reflecting surface was recorded. The expected degree of error in the angle measurements was $\pm 3°$. The distance between the speaker and the microphone was fixed at 1.5 m for each measurement. Simultaneously, a second microphone with identical frequency response was used to measure the undisturbed sound. This second microphone was placed at the same relative position and distance from the speaker as the one inserted within the diffracting/reflecting spiral. At all three elevations it was checked that the ''click'' signals reaching both microphones in the absence of the diffracting/reflecting spiral had almost a flat spectrum (with variations between -1.5 and 1.5 dB) within the frequency range studied (1 kHz to 17 kHz). The spectrum of the impulse responses reaching both microphones was calculated automatically for each recording with the aid of a dedicated fast fourier transform card implemented in a Masscomp MC5450 computer. When using the diffracting/reflecting system, the ratio of the spectra of the signals recorded at both microphones was taken to be the frequency transfer function of the diffracting/reflecting spiral.

B. Results

Figure 2 shows the experimental results together with the predictions of the diffraction/reflection model when evaluated numerically for a collection of surface elements that describe the same three-dimensional shape and dimensions as of the experimental diffracting/reflecting spiral [see Fig. 1(b)]. For this particular geometry, only the diffracting effect of the frontal aperture [S_1 in Fig. 1(b)] was modeled [i.e., $S_A = S_1$ in Eq. (13)]. In other words, the effects of the open sides S_2 and S_3 of the metallic spiral were not considered. Since the reflecting surface was a rigid metallic one, total reflection was assumed (Landau and Lifshitz, 1959, p. 287; Frey *et al.*, 1982, p. 168).

In the third panel of Fig. 2, the experimental results obtained at $-45°$ are compared with the predictions of the model in two cases: (a) (dashed line) when the implemented model is the one presented in Eq. (13) and (b) (continuous heavy line) when the factor $1/r_{ql}$ is omitted in Eq. (13) (i.e., when attenuation of the diffracted waves with distance is not considered). From those results it is obvious that, regarding the central frequencies of the peaks and the notches, the model's predictions are the same in either case. On the other hand, regarding the amplitude of the spectral features, significantly better results are obtained when no attenuation of diffracted wave with distance is considered. Although this result is only presented for $-45°$ elevation, the same occurs for the other locations tested. The actual explanation as to why this happens remains unknown to the authors. Possible reasons are given in Sec. IV. Perhaps, because the distances within the diffracting/reflecting spiral are (<6 cm) smaller or comparable to the studied wavelengths (>1.8 cm), no attenuation of the diffracted wave with distance needs to be considered.[2] Consequently, in order to have a functional model it was decided to evaluate the model considering no attenuation of the diffracted waves with distance and the subsequent effects that this assumption produces in the general formulation.[3] The predicted results for $+35°$, $-17°$, and $-45°$ under this modification are shown in Fig. 2.

The arrows in Fig. 2 show the cancellation frequencies as predicted by the single-delay-and-add formulation for this reflector.[4] Table I shows the frequency position of the experimental minima and the predictions of both the single-delay-and-add approximation and the diffraction/reflection model. The square of the difference between the experimen-

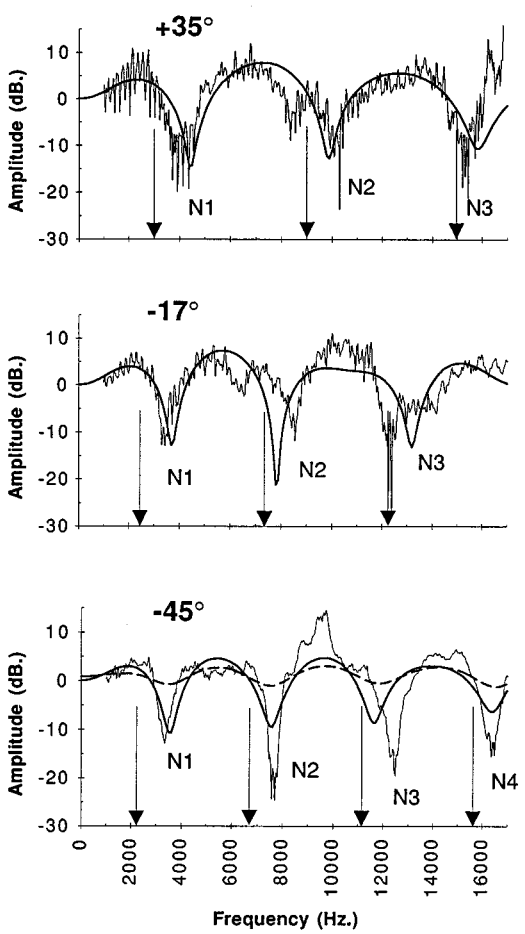

FIG. 2. A comparison of the experimental data with the predictions of the single-delay-and-add approximation and the proposed diffraction/reflection model at three elevations (−45°, −17°, and +35°), for a metal spiral-shaped reflecting surface whose dimensions are shown in Fig. 1(b). The thin continuous line shows the experimental results. The heavy line shows the predictions of the diffraction/reflection model when no attenuation with distance of the diffracted wave is considered. The heavy dashed line in the third panel (−45° elevation) shows the predictions of the diffraction/reflection model when attenuation with distance of the diffracted wave is considered. The arrows indicate the cancellation frequencies as predicted by the single-delay-and-add approximation for the metallic spiral.

tal and the modeled results is calculated for each elevation and each spectral notch as a quantitative estimate of the discrepancy between experimental values and the predictions of both models. For each elevation, the sum of the squared differences is considered to be an indication of the overall performance of the models; that is, the smaller the sum, the better the agreement between experimental and modelled results. The analysis was confined to spectral notches because, as opposed to spectral peaks, they are very narrow and, therefore, their center frequency is very well defined. The outcome of this analysis is that the diffraction/reflection model is more accurate at predicting the frequency position of each one of the examined spectral notches with the only exception of N3 at −17° elevation. But even at this elevation the overall performance of the diffraction/reflection model is better than that of the single-delay-and-add approximation.

It is also remarkable that the single-delay-and-add approximation would predict higher-order notches at frequencies $f_n = n f_1$ $(n = 1,3,5,7,\ldots)$, where f_1 is the frequency of the first notch. At −45°, for example, the first experimental notch is placed at $f_1 = 3.3$ kHz and, therefore, according to the previous formula, the higher-order successive minima should be at: $f_3 = 9.9$ kHz, $f_5 = 16.5$ kHz, and $f_7 = 23.1$ kHz. Experimental results show that these minima actually occur at $f_3 = 7.6$ kHz, $f_5 = 12.3$ kHz, and $f_7 = 16.4$ kHz. These figures clearly indicate that the single-delay-and-add approximation is inadequate to predict both the absolute position of the spectral minima and the relative position between them.

TABLE I. Comparison between the central frequency of the experimental (Exp.) notches observed in the transfer function of the metallic spiral-shaped system (see Fig. 2) and the predictions of the single-delay-and-add (SDAA) approximation and the diffraction/reflection (DR) model. All values are expressed in kHz. The squared difference (d^2) between the experimental values and the predictions of both models is also shown. For every angle of elevation the sum of the squared differences is regarded as an indication of the overall performance of each model.

Elev. +35°	Exp.	SDAA	DR	d^2 (Exp-SDAA)	d^2 (Exp-DR)
N1	4.0	3.0	4.5	1.0	0.25
N2	10.2	9.0	9.8	1.44	0.16
N3	15.5	15.0	15.8	0.25	0.09
			Sum	2.69	0.5
Elev. −17°	Exp.	SDAA	DR	d^2 (Exp-SDAA)	d^2 (Exp-DR)
N1	3.4	2.45	3.75	0.9025	0.1225
N2	8.5	7.35	7.8	1.3225	0.49
N3	12.3	12.25	13.2	0.0025	0.81
			Sum	2.2275	1.4225
Elev. −45°	Exp.	SDAA	DR	d^2 (Exp-SDAA)	d^2 (Exp-DR)
N1	3.3	2.24	3.5	1.1236	0.04
N2	7.6	6.72	7.5	0.7744	0.01
N3	12.3	11.2	11.7	1.21	0.36
N4	16.4	15.68	16.4	0.5184	0.0
			Sum	3.6264	0.41

1. Two-dimensional approximation

To find an approximation for two-dimensional waves, the diffraction/reflection model was also evaluated for the two-dimensional projection of the metal spiral [i.e., for a contour such as the one shown in Fig. 1(a)]. The surface integrals over S_A and S_R become, therefore, line integrals under this approximation. In order to get almost identical results for both the two-dimensional approximation and the real three-dimensional evaluations it was found that the reflection obliquity factor in the two-dimensional case needed to be $\mathbf{R}(r_q, \gamma_q) = \cos \gamma_q$ instead of the theoretical expression given in Eq. (11). This finding will be used when applying the model for the realistic concha contour (see Sec. III).

III. RESULTS FOR A REALISTIC CONCHA SHAPE

In this section the predictions of the diffraction/reflection model for a realistic concha shape are compared against experimental head-related transfer functions (HRTFs). First, experimental data are presented. The method employed for obtaining the experimental HRTFs is explained. The elevation and azimuth dependency of the most characteristic spectral notches is systematically studied. References to other studies are given to support the generality of

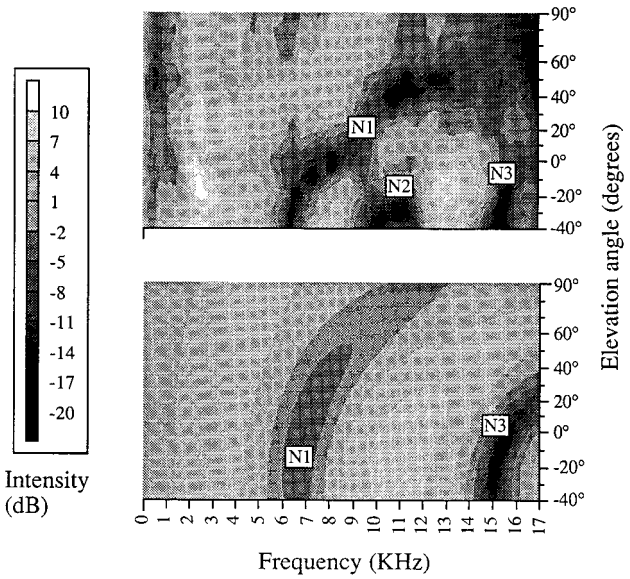

FIG. 3. Top: HRTFs measured at the left eardrum of a KEMAR (pinna model DB-061) as a function of the elevation angle of a sound source placed in the median vertical plane. The spectra were obtained by performing a Fourier analysis on the time domain head-related impulse responses released by Gardner and Martin (1995) (see text for details). The intensity is expressed in dB by the gray scale. The data include the effect of all the body parts which modify the incident sound before it reaches the eardrum, i.e., torso, head, and the whole of the external ear. Bottom: Predictions of the diffraction/reflection model for a realistic concha shape (see main text for details). Only the spectral features associated with the transverse dimensions of the concha are plotted in this panel.

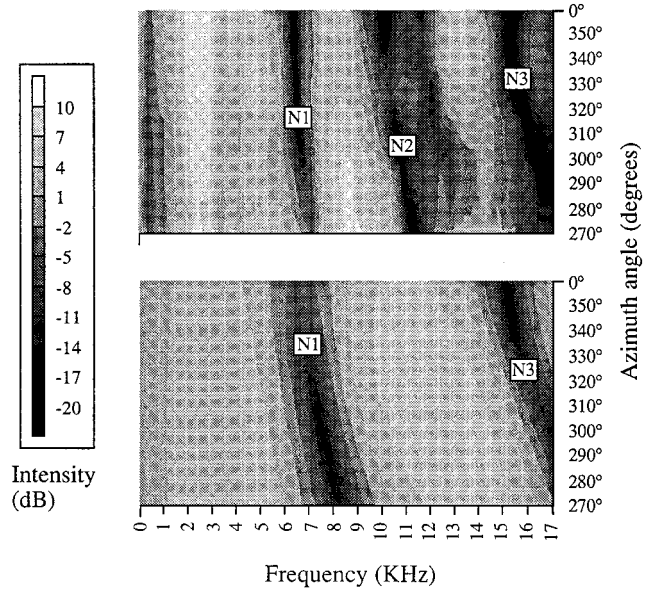

FIG. 4. Top: HRTFs measured at the left eardrum of a KEMAR (pinna model DB-061) as a function of the azimuth angle for a sound source placed at −40° elevation. The angles 270° and 0° correspond to sound sources on the left of the manikin and right ahead, respectively. The intensity is expressed in dB by the gray scale. The spectral data were generated as explained in Fig. 3 and, therefore, the same general comments are applicable in this case. Bottom: The predictions of the diffraction/reflection model for a realistic concha shape (see main text for details).

the experimental results presented here. Then, the predictions of the diffraction/reflection model are compared with these experimental results.

A. Experimental methods and results

1. Experimental method

The experimental HRTFs presented in the top panels of Figs. 3 and 4 were obtained after performing a frequency analysis of the Head-Related Impulse Responses (HRIRs) measured by Gardner and Martin (1995) using a Knowles Electronics Manikin for Acoustic Research (KEMAR). The experimental method for measuring the HRIRs has, therefore, been explained elsewhere (Gardner and Martin, 1995). As advised by Gardner and Martin, the KEMAR head-related impulse responses were reduced to 512 samples (sampling rate 44.1 kHz). The frequency analysis of the impulse responses was then performed using a Macintosh computer (Quadra 660AV) with the aid of the sound processing package SoundEdit Pro. The fast Fourier transform (FFT) function of this package was applied to the reduced impulse responses with the following settings: gain=0 dB, offset=16 pts, size=256 pts, window=Hamming, frequency range: from 0 to 17 kHz. The amplitude of the resulting spectra, $A(f)$, was then expressed in decibels as follows: $\mathrm{dB}(f)=20\log_{10}(A(f))$. The same frequency analysis was performed on the impulse response of the delivering system employed by Gardner and Martin. The HRTFs were then calculated by subtracting the response of the delivering system (expressed in dB) from each one of the analyzed head-related impulse responses.[5]

2. Elevation dependency

Figure 3 (top panel) shows the experimental HRTFs recorded at the left eardrum of the KEMAR with the pinna in place (Ear model: DB-061). The experimental data show clearly the presence of a notch (N1) whose frequency position varies between 6.5 and 10.5 kHz for elevation angles between −40° and +40°, just like the notch described by Shaw and Teranishi (1968) in the lateral vertical plane, and Hebrank and Wright (1974) in the median plane. Additionally, there is another notch (N2), centered at 10.8 kHz, only present at elevations lower than −10°. Finally, a third minimum (N3) appears at around 14 to 17 kHz whose central frequency varies slightly with elevation. For elevation angles greater than +40° the spectral shape is more like a gradual slope decreasing noticeably at high frequencies. The latter result is consistent with the spectra reported by Searle *et al.* (1975, Fig. 2).

3. Azimuth dependency

The azimuthal variation of the spectral notches described above (N1, N2, and N3) is shown in the top panel of Fig. 4. The data correspond to measurements at the left eardrum of the KEMAR (Ear model: DB-061) for an elevation angle of −40° and azimuthal positions between 270° (source on the left) and 0° (source right ahead). Note that there is a slight dependence of N1, N2, and N3 on the azimuthal position of the source: all three minima move slightly toward

higher frequencies as the source moves from the median to the lateral planes. Despite this dependence on azimuth, the three notches are present for sources placed at all vertical planes within the frontal part of the ipsilateral hemisphere. Indeed, data from the same set of HRTFs not shown here confirm that the central frequency of N1, N2, and N3 varies similarly with elevation in any vertical plane within the azimuthal positions studied. Moreover, even for sound sources in the frontal part of the contralateral side, the same spectral pattern has been observed (in particular, N1 and N3 appear very clearly and show the same dependence on elevation as for incident sounds from the ipsilateral side). Notice that these results agree with the fact that similar elevation-dependent spectral notches have been reported in the lateral and median vertical planes in different studies [in the lateral vertical plane: Shaw and Teranishi, 1968; Bloom, 1977; Carlile and Pralong, 1994, Fig. 5(b); in the median vertical plane: Hebrank and Wright, 1974; Butler and Belendiuk, 1977; Carlile and Pralong, 1994, Fig. 5(a)].

4. Generalization of these results to human HRTFs

The slight azimuthal variation of N1 is not peculiar to the KEMAR ears and has also been observed in human HRTFs (Mehrgardt and Mellert, 1977, Figs. 11 and 12; Carlile and Pralong, 1994, Fig. 4; Pralong and Carlile, 1994, Fig. 3). In Carlile and Pralong's human HRTFs, there is a spectral notch (possibly corresponding to N1) whose central frequency varies from around 6 kHz when the source is in the median vertical plane to 7.5 kHz when the source is in the lateral vertical plane at 0° elevation. Pralong and Carlile present human HRTFs which show a spectral notch (possibly N1) whose central frequency hardly deviates from 7 kHz when the source moves from the median vertical plane to the lateral plane at 0° elevation. It is worth noticing that the HRTFs presented in those reports were recorded at 0° elevation and this may be the reason why N2 is either not present for all source azimuths or its azimuthal dependency is more variable than that observed in Fig. 4 for the KEMAR.

Another example of the slight azimuthal variation of N1 is shown in Fig. 5. These HRTFs were recorded in our laboratory also using a KEMAR. However, in our experiments the KEMAR was not fitted with standard Knowles pinnae but with pinnae molded from the left and right ears of three subjects.[6] The experimental procedure for measuring the HRTFs was similar to that used when measuring the impulse response of the diffracting/reflecting spiral (see Sec. II A above). Measurements were made every 5° for source azimuths between 270° and 90° at −40° elevation in the frontal hemisphere (notice that Fig. 5 only shows the HRTFs at left ear for source azimuths between 270° and 0°). Even though the data shown in Fig. 5 correspond to the molded left pinna of one subject, similar spectral features are observed for each and every one of the other five molded pinna tested. Particularly the slight azimuthal variation of the N1 for an ipsilateral sound source is a characteristic of all six HRTFs examined in this experiment.

The pronounced elevation dependency and the slight azimuth dependency of the spectral notches (in particular of N1) described above seem to be, therefore, a general feature

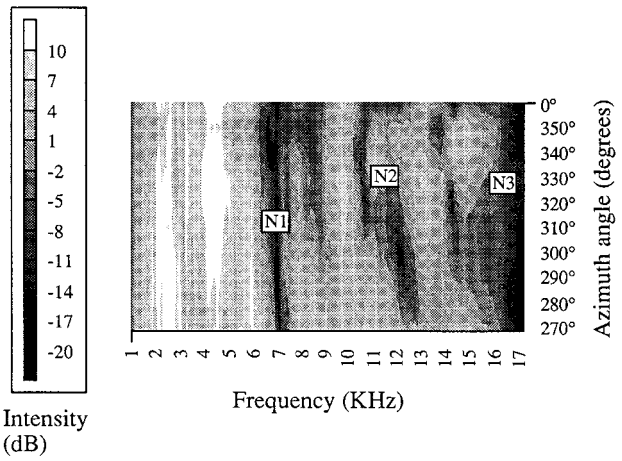

FIG. 5. HRTFs measured at the left eardrum of a KEMAR as a function of source azimuth for a sound source placed at −40° elevation and azimuth angles between 270° and 0°. The pinna used in this experiment was not DB-061 but was molded from a subject's ear and adequately fitted on the KEMAR. Although the results presented in this figure were obtained with a different recording method and using a different pinna from those presented in the top panel of Fig. 4, the spectral characteristics are very similar in both cases.

of all HRTFs measured using humanlike or real human ears. In the next section it is examined whether the diffraction/reflection model is able to predict spectral notches with a similar azimuth- and elevation-dependent behavior.

B. Predictions of the diffraction/reflection model

The diffraction/reflection model was evaluated for an approximated concha shape with a geometry such that the spectral features related to the transverse dimensions of the human concha should be predicted. In order to generate such a shape, the inner contour [Fig. 6(a)] of a molded concha was measured from the center of the ear-canal entrance to its posterior wall. An approximate three-dimensional shape was then generated by projecting the contour to a vertical plane oriented at a protrusion angle (Burkhard and Sachs, 1975) of 158° with respect to the frontal part of the median sagittal plane [Fig. 6(b)]. The resulting geometry is an approximate concha cavity defined by the lateral reflecting wall, S_L, the posterior reflecting wall, S_P, and the diffracting aperture, S_A (see Fig. 6). The dimensions of the concha breadth (≈1.8 cm), concha depth (≈1.33 cm), and protrusion angle (158°) in the approximate concha are close to the average values for a male ear reported by Burkhard and Sachs (1975).

Although reflections from the lateral wall are also considered in the general formulation of the diffraction/reflection model, their contribution to the reflected pressure at the meatus entrance is zero for the approximate concha considered in this case. The reason is that $\gamma_q = 90°$ for all surface elements in S_L and, therefore, the factor $\cos \gamma_q$ in the reflection obliquity factor [Eq. (11)] becomes zero over the lateral wall. Consequently, the integration over the reflecting surface in the diffraction/reflection model was evaluated over the posterior wall only. The evaluation of the diffraction/reflection model under these conditions should predict the

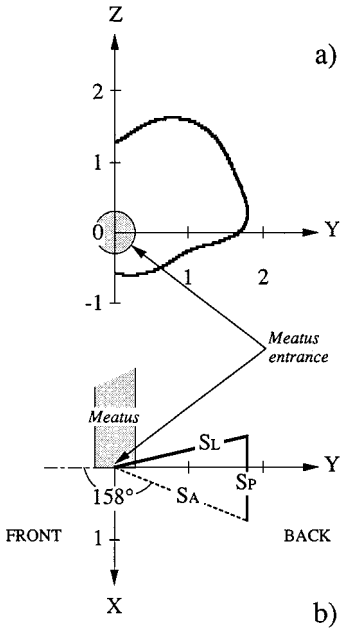

FIG. 6. (a) The inner contour (lateral view or YZ projection) of a real concha which was used to generate the approximate 3D-concha shape for which the diffraction/reflection theory has been evaluated. (b) Top view (or XY projection) of the approximate three-dimensional concha. Note that the protrusion angle is 158° and that the concha cavity is effectively described by two reflecting surfaces (S_L and S_P) and by the diffracting aperture S_A. The axes units are given in cm and express to scale the real dimensions of the concha.

spectral features related to the transverse dimensions of the concha.

The bottom panels of Figs. 3 and 4 show the predictions of the diffraction/reflection model when it is applied to the approximate concha shape for the same sound-source positions as those considered in the experimental data. As for the metal reflecting spiral, the amplitude of the predicted spectral features (peaks and notches) was very much smaller than the experimental values. In order to improve the predicted amplitudes, attenuation with distance of neither the diffracted nor the reflected waves was considered in this case. What is more, although the model was applied to a three-dimensional reflecting surface, the two-dimensional reflection obliquity factor, $\mathbf{R}(r_q, \gamma_q) = \cos \gamma_q$, was used so that the amplitude of the reflected wave was larger. For the realistic concha, therefore, the diffraction/reflection model was evaluated using these modifications, whose theoretical implications will be discussed below. Moreover, the model was evaluated assuming total reflection.

The diffraction/reflection model predicts the location of notches N1 and N3 and the dependence of their central frequency on the elevation and azimuthal angles. With the modifications explained above, the depth of N1 and N3 is comparable to the experimental values for most azimuths and elevation angles between $-45°$ and $+45°$. However, in the median plane the predicted depth of N1 (-9 dB maximum) is still smaller than the experimental values presented in this paper (which are of the order of -15 to -20 dB maximum). The modeled data also anticipate that N1 is deeper at elevations around 0° for any vertical plane. This prediction coincides with the experimental data shown in this paper and the data reported by Shaw and Teranishi (1968) and Bloom (1977). For elevations higher than $+45°$, an individual analysis of the predicted spectra shows that the modeled N1 appears at higher frequencies (around 16 kHz for $+90°$) and is much wider than at low elevations. This may be why the experimental spectra appear like a gradually decreasing slope for elevation angles close to $+90°$. Even with the modifications explained above, the depth of the predicted notches at elevations higher than $+45°$ is very much smaller than the experimental values (see Fig. 4) for any azimuthal angle. The model does not simulate the experimental notch N2. Instead, it predicts a resonance between 10 and 13 kHz which corresponds to the transverse mode of resonance of the concha, or vertical mode (Shaw, 1975).

IV. DISCUSSION

The experimental HRTFs are more irregular than the model results. A reason for this dissimilarity is that, while the modeled results only reflect the spectral features generated by the posterior wall of a simplified concha, the experimental data also include the effects of the concha depth, head, torso, pinna flange, helix, tragus, ear canal, and other anatomical parts of the human pinna. All of these parts also contribute to the final spectra recorded at the eardrum (Teranishi and Shaw, 1968; Shaw, 1975). Additionally, the model has been evaluated assuming ideal total reflection, even for the real concha. Obviously, this is not the real case. Unfortunately, no precise data about the acoustic properties of the material used to make the manikin's ears were available when carrying out these studies.

For sounds incident from the median plane, the diffraction/reflection model supports Hebrank and Wright's speculation that notch N1 is caused by cancellation between the direct sound entering the meatus and the reflected wave from the posterior wall of the concha. However, in the diffraction/reflection theory reflections from the whole of the concha's posterior wall have been considered. Therefore, the dependence of N1 and N3 on elevation must be the result of the asymmetry of the reflecting wall with respect to the meatus entrance, together with the weighting of the amplitudes for the multiple delays which is given (as explained in the theory) by the obliquity factors for diffraction and reflection.

The most important feature of the diffraction/reflection theory is, perhaps, that it simulates and explains why similar spectral features (in particular, N1 and N3) have been observed when the sound source is placed in any vertical plane within the frontal hemisphere. In other words, it simulates the slight dependence of the central frequency of N1 and N3 on the azimuthal position of the sound source. The explanation is as follows: Whatever the incident direction (source position), the diffraction process scatters the sound within the concha cavity. Consequently, reflections on the posterior wall of the concha occur for any incident direction of the sound (although the diffraction obliquity factor encourages sounds coming from the frontal part of the ipsilateral hemisphere). Interference between the direct and reflected waves at the meatus entrance generates, therefore, a similar spectral pattern whatever the azimuthal angle of the sound source.

Even for sources placed in the frontal part of the contralateral side, the same mechanism applies if we accept that the sound ''creeps'' around the head entering the contralateral concha at *approximately* the same elevation angle as if the source was in the ipsilateral hemisphere. However, when the sound source is off the median plane, the effect of the head must also be taken into account to evaluate the amplitude of the individual frequency components of the signal reaching the concha aperture.

The reason N1 should be deeper at elevations around 0° is also explained by the diffraction/reflection model. From Eq. (13) it is obvious that deeper notches must occur for elevation angles, ϕ, at which the normalized amplitude of the reflected wave is closer to unity. The only direction-dependent factor in the amplitude of the reflected wave is the diffraction obliquity factor, $\mathbf{K}(\theta_{ql},\psi_l,r_{ql})$ [Eq. (8)]. The other factors only depend on the geometry of the problem. Therefore, maximum reflected amplitudes are obtained for elevation angles at which **K** is maximal. From Fig. 1(a)[7] it can be seen that $\cos\theta_{ql}$ is direction-independent and $\cos\psi_l=-\cos\phi$. Consequently, at 0° elevation $\cos\psi_l=-1$ and, therefore, $\mathbf{K}(\theta_{ql},\psi_l,r_{ql})$ reaches its maximum value with respect to ϕ.

Regarding the amplitude of the simulated spectra, certain modifications (listed above) have been introduced in the model in order to generate spectral features whose amplitudes are comparable to the experimental values. The main effect of introducing such modifications is an overall increase of the amplitude of the reflected wave (i.e., the amplitude of $\mathbf{p_R}/\mathbf{p_0}$) which, therefore, generates higher peaks and deeper notches at those frequencies at which the phase of the reflected wave is close to 0 and π rads, respectively. It is important to notice that those modifications do not modify the dependence of the central frequency of the predicted features on the incident direction of the sound, which is included in the model by the initial phase φ_l and the angle ψ_l. A robust theoretical argument which explains why those modifications are required is not known by the authors, but it is most likely a consequence of the approximations made for developing the diffraction/reflection transfer function. It is important to notice that the single-reflection approximation (iv) yields a reflected wave whose amplitude is slightly smaller than the value it would have if the approximation were not assumed (i.e., if multiple reflections were considered). It may also be that, in the case of the real concha, the size of the diffracting and reflecting surfaces and the distance between them is so small compared to the wavelength that attenuation with distance does not need to be considered at all.[8]

Even with the adjustments explained above, results have shown that for elevation angles greater than around +40°, N1 is less deep in the model than in the experimental data. This may be partially explained because Kirchhoff's theory of diffraction does not work very accurately for angles of incidence far away from the normal to the diffracting aperture (Braddick, 1965; p 176). In addition, in the real case, the pinna flange must cause some important ''shadow effect'' for sounds coming from high elevations.

The diffraction/reflection model presented here cannot simulate the minimum at 10.5 kHz (N2). It may well be caused by an anatomical part of the real pinna not considered in the model or it may be related to other physical phenomena than those related to the transverse dimensions of the concha. The fact that it is right in the middle of the predicted vertical resonance of the concha indicates that it may be caused by the presence of the crus helias and the fossa in the real concha, as Shaw (1975) observed.

V. CONCLUSIONS

An approximated physical model of sound diffraction and reflections in the human concha has been proposed. The model constitutes, to our knowledge, the first attempt ever to include diffraction in the formulation. Results are promising regarding the predictions of the center frequency of some of the most characteristic spectral notches. However, some modifications in the theoretical formulation of the diffraction/reflection model have been required in order to optimize the amplitude of the predicted spectral features. These modifications only increase the depth of the predicted minima and do not change their central frequencies or their dependence on source location. The need for these modifications is likely to be a direct consequence of the approximations made when developing the diffraction/reflection model of the concha.

Although the proposed diffraction/reflection model accounts for some of the spectral features related to the transverse dimensions of the concha, it is only an approximation. Further investigation needs to be done in two different directions in order to predict a complete functional model of the human concha. First, a general formulation which needs no major assumptions and approximations should be developed. Second, the improved formulation should be adequate to explore in a unified manner the spectral features originated by both the depth of the concha and its transverse dimensions, and by the interactions between them. This could only be achieved by solving, for each source location, the wave equation with the right boundary conditions for an acoustic system such as the concha and, perhaps, the ear.

ACKNOWLEDGMENT

This research was supported by a grant from the Image Interpretation Initiative of the Science and Engineering Research Council, UK (GR/H/52634).

APPENDIX

A general solution for the wave equation in a bounded or unbounded medium with no sound sources is given by Morse and Ingard (1968):

$$\mathbf{p}(\overline{r})=\int\int_S [g(\omega,R_0)\boldsymbol{\nabla}_0\mathbf{p}(\overline{r_0}) - \mathbf{p}(\overline{r_0})\boldsymbol{\nabla}_0 g(\omega,R_0)]\, ds_0, \tag{A1}$$

where $R_0=|\overline{r}-\overline{r_0}|$ and the integration is done over any closed surface, S, which surrounds the observation point $\overline{r}$. $g(\omega,R_0)$ is the Green's function whose value is

$$g(\omega,R_0)=\frac{\exp(jkR_0)}{4\pi R_0}. \tag{A2}$$

Equation (A1) essentially states that in order to know the value of the sound pressure at the observation point $\overline{r}$, the value of the pressure and its gradient through any closed surface surrounding the observation point need to be known. Notice that $\nabla_0 g(\omega,R_0)$ in Eq. (A1) can be expressed as

$$\nabla_0 g(\omega,R_0)=\cos\ \gamma_0\ \frac{\partial}{\partial R_0}\ g(\omega,R_0)$$

$$=\cos\ \gamma_0\left(jk-\frac{1}{R_0}\right)g(\omega,R_0), \tag{A3}$$

where $\overline{n_0}$ is the unit vector normal to the surface (defined pointing outwards) and $\gamma_0=\text{angle}(\overline{n_0},\overline{R_0})$, with $\overline{R_0}=\overline{r_0}-\overline{r}$.

1. Diffracted pressure at any point behind the aperture

Equation (A1) is the main result used to derive Kirchhoff's theory of diffraction and its approximation[9] to obtain the diffracted pressure behind apertures (Braddick, 1965; Ditchburn, 1976; Hecht, 1990). For an incident plane wave of the form shown in Eq. (3), the value of $\nabla_0\mathbf{p}(\overline{r_0})$ can be expressed as

$$\nabla_0\mathbf{p}(\overline{r_0})=jk\ \cos(\overline{n_0},\overline{k})\mathbf{p}(\overline{r_0}). \tag{A4}$$

The diffracted pressure at any point behind the aperture [i.e., Eq. (6)] is obtained by substituting Eqs. (A2), (A3), and (A4) and the value of the incident plane wave at each point on the aperture into Eq. (A1). The expression for the diffraction obliquity factor, **K**, emerges naturally from the calculations. The observation points, in our particular case, are all the points on the reflecting surface (i.e., $\overline{r}=\overline{r_q}$, $\forall\overline{r_q}\in S_R$). For the case of diffraction by an aperture, the integration surface, S, becomes the surface of the aperture, S_A, and the zero subscript, which refers to a general arbitrary surface, must be substituted by the subscript l, which specifically refers to S_A. Therefore, the vector $\overline{R_0}=\overline{r_0}-\overline{r}$ reduces to $\overline{r_{ql}}$, the angle γ_0 becomes θ_{ql} and $\cos(\overline{n_0},\overline{k})=\cos\ \psi_l$ [see Fig. 1(a)].

2. Reflected pressure from the reflecting wall

The general result expressed in Eq. (A1) has been also applied to obtain the reflected pressure from the concha reflecting surface [i.e., to obtain Eq. (10)]. However, in this case, the integration must be done over the reflecting surface, S_R, and boundary conditions on the surface must be applied. In addition, the subscript zero must be substituted by q, which specifically refers to S_R. The observation point for the reflection process is the meatus entrance, which, for convenience, has been defined at the origin of the system of coordinates (i.e., $\overline{r}=0$). Therefore, $\overline{R_0}=\overline{r_0}$ which has been named $\overline{r_q}$ in our case [see Fig. 1(a)].

If the reflecting surface is such that total reflection can be assumed (i.e., it is perfectly rigid), the boundary condition is that the normal component of the particle velocity must be zero at the reflecting surface (Morse and Ingard, 1968, p. 366). This condition is held if, and only if,

$$\nabla_q\mathbf{p}(\overline{r_q})=0. \tag{A5}$$

Therefore, with the above considerations, Eq. (A1) reduces to

$$\mathbf{p_R}=-\int\int_{S_R}[\mathbf{p}(\overline{r_q})\nabla_q g(\omega,r_q)]\ ds_q. \tag{A6}$$

The previous expression requires the value of the total pressure field on the reflecting surface [i.e., $\mathbf{p}(\overline{r_q})$] to be known. In our case, $\mathbf{p}(\overline{r_q})$ has been approximated as the diffracted pressure on the reflecting surface, $\mathbf{p_D}(\overline{r_q})$ [approximation (iv)]. Under this assumption, the reflected pressure at the meatus entrance can be obtained by substituting Eq. (A3) into (A6). The expression for the reflection obliquity factor for the case of total reflection [Eq. (11)], $\mathbf{R}(r_q,\gamma_q)$, is obtained trivially from the calculations as

$$\mathbf{R}(r_q,\gamma_q)=-\frac{\nabla_q g(\omega,R_q)}{4\pi\cdot g(\omega,R_q)}=\frac{\cos\ \gamma_q}{4\pi}\left(\frac{1}{r_q}-jk\right). \tag{A7}$$

If the reflecting surface is not perfectly rigid but is still passive, the boundary condition is no longer the one given by Eq. (A5) but (Morse and Ingard, 1968):

$$\nabla_q\mathbf{p}(\overline{r_q})=j\omega\rho_q\frac{\mathbf{p}(\overline{r_q})}{\mathbf{Z}_N(\overline{r_q},\omega)}, \tag{A8}$$

where $\mathbf{Z}_N(\overline{r_q})$ is the normal acoustic impedance of the surface and ρ_q is the density of the reflecting material. $\mathbf{Z}_N(\overline{r_q})$ is defined as the ratio between the pressure and the normal component of the particle velocity at the reflecting surface, i.e.,

$$\mathbf{Z}_N(\overline{r_q})=\frac{\mathbf{p}(\overline{r_q})}{\mathbf{u}_N(\overline{r_q})}. \tag{A9}$$

For real materials, $\mathbf{Z}_N(\overline{r_q})$ varies with the frequency of the incident sound wave.

Substituting Eq. (A8) into Eq. (A1), considering approximation (iv) and operating, we obtain an *approximate* value for the total reflected pressure at the origin:

$$\mathbf{p_R}=\int\int_{S_R}\left\{\mathbf{p}(\overline{r_q})g(\omega,r_q)\right.$$

$$\left.\times\left[\frac{j\omega\rho_q}{\mathbf{Z}_N(\overline{r_q})}-\cos\ \gamma_q\left(jk-\frac{1}{r_q}\right)\right]\right\}\ ds_q. \tag{A10}$$

In this case, the reflection obliquity factor is

$$\mathbf{R}(r_q,\gamma_q,\mathbf{Z}_N)=\frac{j\omega\rho_q}{4\pi\mathbf{Z}_N(\overline{r_q})}-\frac{\cos\ \gamma_q}{4\pi}\left(jk-\frac{1}{r_q}\right). \tag{A11}$$

Now $\mathbf{R}(r_q,\gamma_q,\mathbf{Z}_N)$ not only depends on the geometry of the problem but also on the acoustic properties of the reflecting surface. Note that when $\mathbf{Z}_N=\infty$ (i.e., total reflection), the value of $\mathbf{R}(r_q,\gamma_q,\mathbf{Z}_N)$ reduces to $\mathbf{R}(r_q,\gamma_q)$, as it should happen.

[1]The contour of the metallic reflector in the YZ plane is described by a collection of pairs (y,z) which are expressed as $y=C\beta\cos(\beta+\pi/2)$ and $z=C\beta\sin(\beta+\pi/2)$, where β is the angle (in radians) with respect to the

positive Y axis and C is a constant. In our case $C=0.676$. Therefore, the metallic diffracting/reflecting surface is, in fact, a spiral of radius $r=C\beta$, rotated an angle $\pi/2$, where only the values $\pi \leqslant \beta \leqslant 2\pi$ are considered. In the experimental setup the microphone was placed at the centre of the spiral.

[2]Stephens and Bate (1966) obtained correct results when describing the diffraction by a single slit even though they tacitly omitted the attenuation with distance of the diffracted waves. They justified their assumption by the correct results that it yielded.

[3]A immediate consequence of not considering attenuation of the diffracted waves is that the imaginary part of Kirchoff's obliquity factor disappears from Eq. (8). This can be demonstrated noticing that, when attenuation with distance of the diffracted wave is not considered, the Green's function [Eq. (A2)] for the diffracting surface becomes

$$\tilde{g}(\omega,R_0)=\exp(jkR_0)/4\pi,$$

and, therefore, the gradient through the diffracting aperture is no longer as shown in Eq. (A3), but

$$\nabla_0\tilde{g}(\omega,R_0)=jk\cos\gamma_0\tilde{g}(\omega,R_0).$$

The resulting Kirchoff's obliquity factor after substituting this expression into Eq. (A1) and operating is equal to the real part of Eq. (8).

[4]According to the classical theory of concha reflections, for sounds incident from the median plane the cancellation frequencies are given by $f_n=n(1/2\tau(\phi))$ where $n=1,3,5,...$, and $\tau(\phi)=d/c$. In this case, the path difference between the direct and reflected waves, d, was calculated as $d=2r$, where r is the distance from the microphone to the point on the reflecting wall at which the sound would reflect if it traveled within the cavity keeping its original direction (i.e., keeping its original elevation).

[5]The microphone (Neumann KMi 84) used to measure the impulse response of the delivering speaker (Optimus Pro) was different from that used to measure the KEMAR head-related impulse responses (Etymotic ER11) (see Gardner and Martin, 1995). Consequently, the difference response between both microphones is not accounted for in the analysis process and is certainly included in the presented HRTFs.

[6]A detailed description of the pinna-molding procedure goes beyond the purpose of this paper. Detail information on this procedure can be found in the following World Wide Web address: http://info.lut.ac.uk/departments/hu/groups/speechlab/pinnae_modelling.html.

[7]It should be noticed that, although the real system is three-dimensional, the two-dimensional description given in Fig. 1(a) is enough to illustrate the dependence of **K** on elevation.

[8]Only at distances large compared with the size of the source and with the wavelength is the flow of energy proportional to the inverse square of the distance from the source (Ditchburn, 1976, p. 25).

[9]Kirchhoff's analysis applies to an integral taken over the whole of a closed surface which surrounds the point at which we are interested in finding the diffracted wave. When an obstacle is inserted (for instance, an infinitely large opaque screen in which there is an aperture), the pressure field at the point of interest can be calculated by integrating over the unobstructed part of the wavefront, i.e., over the surface of the aperture. This approximation is normally known as St. Venant's hypothesis (Ditchburn, 1976, p. 174).

Batteau, D. W. (**1967**). ''The role of pinna in human localization,'' Proc. R. Soc. London Ser. B **168**, 158–180.

Bloom, P. J. (**1977**). ''Determination of monaural sensitivity changes due to the pinna by use of minimum-audible-field measurements in the lateral vertical plane,'' J. Acoust. Soc. Am. **61**, 820–828.

Braddick, H. J. J. (**1965**). *Vibrations, Waves, and Diffraction* (McGraw-Hill, London).

Burkhard, M. D., and Sachs, R. M. (**1975**). ''Anthropometric manikin for acoustic research,'' J. Acoust. Soc. Am. **58**, 214–222.

Butler, R. A., and Belendiuk, K. (**1977**). ''Spectral cues utilized in the localization of sound in the median sagittal plane,'' J. Acoust. Soc. Am. **61**, 1264–1269.

Carlile, S., and Pralong, D. (**1994**). ''The location-dependent nature of perceptually salient features of the human head-related transfer functions,'' J. Acoust. Soc. Am. **95**, 3445–3459.

Cassot, F. (**1975**). ''Contribution à l'étude de la diffraction par un écran mince,'' Acustica **34**, 64–71.

Ditchburn, R. W. (**1976**). *Light* (Academic, London).

Filippi, P., and Dumery, G. (**1969**). ''Etude théorique et numérique de la diffraction par un ecran mince,'' Acustica **21**, 343–350.

Frey, A. R., Coppens, A. B., and James, V. S. (**1982**). *Fundamentals of Acoustics* (Wiley, New York), Chap. 8.

Gardner, B. and, Martin, K. (**1995**). ''HRTF measurements of a KEMAR,'' J. Acoust. Soc. Am. **97**, 3907–3908. Database available via anonymous ftp at sound.media.mit.edu, under pub/Data/Kemar (Internet address 18.85.0.105).

Hebrank, J., and Wright, D. (**1974**). ''Spectral cues used in the localization of sound sources on the median plane,'' J. Acoust. Soc. Am. **56**, 1829–1834.

Hecht, E. (**1990**). *Optics* (Addison-Wesley, New York), 2nd ed., Chap. 10.

Landau, L. D., and Lifshitz, E. M. (**1959**). *Fluid Mechanics*, in the series Course of Theoretical Physics (Pergamon, New York), Vol. 6, Chap. 8.

Martin, P. A., and Rizzo, F. J. (**1989**). ''On boundary integral equations for crack problems,'' Proc. R. Soc. London Ser. A **421**, 341–355.

Mehrgardt, S., and Mellert, V. (**1977**). ''Transformation characteristics of the external human ear,'' J. Acoust. Soc. Am. **61**, 1567–1576.

Mills, A. W. (**1972**). ''Auditory Localization'' in *Foundations of Modern Auditory Theory*, edited by J. V. Tobias (Academic, New York), Vol. 2.

Morse, P., and Ingard K. U. (**1968**). *Theoretical Acoustics* (McGraw-Hill, New York), Chap. 7.

Pralong, D., and Carlile, S. (**1994**). ''Measuring the human head-related transfer functions: A novel method for the construction and calibration of a miniature ''in ear'' recording system,'' J. Acoust. Soc. Am. **95**, 3435–3444.

Searle, C. L., Braida, L. D., Cuddy, D. R., and Davis, M. F. (**1975**). ''Binaural pinna disparity: Another auditory localization cue,'' J. Acoust. Soc. Am. **57**, 448–455.

Shaw, E. A. G. (**1975**). ''The external ear: New knowledge,'' in *Ear Moulds and Associated Problems*, Seventh Danavox Symposium (1975). Gl. Avernes, Denmark. Distributed by: The Almquist & Wiksell Periodical Co. Stockholm. Sweden.

Shaw, E. A. G., and Teranishi, R. (**1968**). ''Sound pressure generated in an external-ear replica and real human ears by a nearby point source,'' J. Acoust. Soc. Am. **44**, 240–249.

Stephens, R. W. B., and Bate, A. E. (**1966**). *Acoustics and Vibrational Physics* (Edward Arnold, London), Appendix 14.

Teranishi, R., and Shaw, E. A. G. (**1968**). ''External-ear acoustic models with simple geometry,'' J. Acoust. Soc. Am. **44**, 257–263.